JOURNAL OF GUIDANCE, CONTROL, AND DYNAMICS
Vol. 30, No. 5, September–October 2007

Adaptive, Integrated Guidance and Control Design for Line-of-Sight-Based Formation Flight

Byoung Soo Kim*
Gyeongsang National University, Gyeongnam 660-701, Republic of Korea
and
Anthony J. Calise† and Ramachandra J. Sattigeri‡
Georgia Institute of Technology, Atlanta, Georgia 30332-0150

DOI: 10.2514/1.27758

This paper presents an integrated guidance and control design for formation flight using a combination of adaptive output feedback and backstepping techniques. We formulate the problem as an adaptive output feedback control problem for a line-of-sight-based formation flight configuration of a leader and a follower aircraft. The design objective is to regulate range and two bearing angle rates while maintaining turn coordination. Adaptive neural networks are trained online with available measurements to compensate for unmodeled nonlinearities in the design process. These include uncertainties due to unknown leader aircraft acceleration, and the modeling error due to parametric uncertainties in the aircraft aerodynamic derivatives. One benefit of this approach is that the guidance and flight control design process is integrated. Simulation results using a nonlinear 6 degrees-of-freedom simulation model are presented to illustrate the efficacy of the approach by comparing the performance with an adaptive timescale separation-based guidance and control design.

Nomenclature

$a_{F_{X,B}}, a_{F_{Y,B}}, a_{F_{Z,B}}$	=	acceleration components of follower aircraft in body-fixed coordinate system
$a_{F_{X,I}}, a_{F_{Y,I}}, a_{F_{Z,I}}$	=	acceleration components of follower aircraft in inertial coordinate system
$\overline{\boldsymbol{a}}_L$	=	acceleration vector of leader aircraft in inertial coordinate system
$a_{X_I}, a_{Y_I}, a_{Z_I}$	=	relative acceleration components in the inertial coordinate system
$\Im_{A_X}, \Im_{T_X}$	=	aerodynamic and thrust force component along x-body axis
f_x	=	specific force along body-fixed x axis
g	=	acceleration due to gravity
$[L_x], [L_y], [L_z]$	=	rotation matrices
$L_{\delta a}$	=	estimated aileron control effectiveness
$M_{\delta e}$	=	estimated elevator control effectiveness
$N_{\delta r}$	=	estimated rudder control effectiveness
p, q, r	=	angular velocity components of follower aircraft in the body-fixed coordinate system
R	=	range between leader aircraft and follower aircraft
R_X, R_Y, R_Z	=	line-of-sight range vector projection along the inertial x, y, and z axes
U, V, W	=	velocity components of follower aircraft in the body-fixed coordinate system
$\overline{\boldsymbol{u}}$	=	control input vector of follower aircraft
$\overline{\boldsymbol{u}}_{\text{ad}}$	=	vector of neural network outputs in azimuth rate backstepping formulation
V_{com}	=	speed command of leader aircraft
$\hat{\boldsymbol{W}}$	=	neural network weight vector
$X_{\delta T}$	=	estimated throttle control effectiveness
$\bar{\boldsymbol{x}}$	=	composite state vector of follower aircraft, including line-of-sight states and rigid-body aircraft states
$\overline{\boldsymbol{y}}$	=	regulated output vector of follower aircraft
$\tilde{y}_R, \tilde{y}_{\dot{\chi}_A}, \tilde{y}_{\dot{\chi}_E}, \tilde{y}_\Phi$	=	reference command tracking errors of the range, azimuth bearing rate, elevation bearing rate, and bank angle control channels, respectively
$\tilde{y}_{\text{ad},R}, \tilde{y}_{\text{ad},\dot{\chi}_A}, \tilde{y}_{\text{ad},\dot{\chi}_E}, \tilde{y}_{\text{ad},\Phi}$	=	training signals for the neural networks in the range, azimuth bearing rate, elevation bearing rate, and bank angle control channels, respectively
$\overline{\boldsymbol{y}}_c^{(r)}$	=	vector of reference model feedforward terms, with vector relative degree r
$\boldsymbol{z}$	=	blended output vector regulated for maintaining turn coordination, $\boldsymbol{z} = \beta + C_r r$
α, β	=	angle-of-attack and sideslip angles
$\bar{\boldsymbol{\Delta}}, \bar{\boldsymbol{\Delta}}_2$	=	composite modeling error vectors for integrated guidance and control-1 and 2 designs, respectively
$\delta T, \delta a, \delta e, \delta r$	=	throttle, aileron, elevator, and aileron deflections, respectively

Presented as Paper 6716 at the AIAA Guidance Navigation and Control Conference and Exhibit, Keystone, Colorado, 21–24 August 2006; received 11 September 2006; revision received 9 April 2007; accepted for publication 26 April 2007.

*Associate Professor, School of Mechanical and Aerospace Engineering; bskim@gsnu.ac.kr. AIAA Member.
†Professor, School of Aerospace Engineering; anthony.calise@ae.gatech.edu. Fellow AIAA.
‡Graduate Research Assistant, School of Aerospace Engineering; gte334x@prism.gatech.edu. AIAA Member.

$\bar{\Lambda}$ = modeling error vector in the backstepping formulation, for the integrated guidance and control-2 design

λ_A, λ_E = elevation and azimuth angles of line-of-sight

$\bar{\nu}$ = pseudocontrol vector in integrated guidance and control-1 design, $\bar{\nu} = [\nu_R \nu_{\dot{\chi}_A} \nu_{\dot{\chi}_E} \nu_\Phi]^T$

$\bar{\nu}_{\text{dc}}$ = vector of linear compensator outputs in integrated guidance and control-1 design, $\bar{\nu}_{\text{dc}} = [\nu_{\text{dc},R} \nu_{\text{dc},\dot{\chi}_A} \nu_{\text{dc},\dot{\chi}_E} \nu_{\text{dc},\Phi}]^T$

$\bar{\nu}_{\text{ad}}$ = vector of adaptive neural network outputs in integrated guidance and control-1 design

$\bar{\nu}_2$ = pseudocontrol vector in integrated guidance and control-2 design, $\bar{\nu}_2 = [\nu_R \nu_{\zeta_3} \nu_{\dot{\chi}_E} \nu_z]^T$

$\bar{\nu}_h$ = vector of pseudocontrol hedge signals in integrated guidance and control-1 design, $\bar{\nu}_h = [\nu_{h,R} \nu_{h,\dot{\chi}_A} \nu_{h,\dot{\chi}_E} \nu_{h,\Phi}]^T$

$\tau_{\dot{\chi}_A}, \tau_{\dot{\chi}_E}$ = time constant of the azimuth bearing and elevation bearing rate reference models

Φ, Θ, Ψ = Euler bank, pitch, and yaw angles

$\boldsymbol{\phi}$ = neural network basis function vector

$\boldsymbol{\phi}_f$ = filtered neural network basis function vector

χ_A, χ_E = bearing angles; $\chi_A = \lambda_A - \Psi$, $\chi_E = \lambda_E - \Theta$

$\omega_{n_R}, \omega_{n_\Phi}, \varsigma_R, \varsigma_\Phi$ = natural frequency and damping ratio of the range and bank angle control reference models

I. Introduction

THE problem of leader–follower formation flight in which the follower aircraft is equipped with only an onboard camera to track the leader aircraft is quite challenging. This problem requires simultaneous sensor data processing, state estimation, and tracking control in the presence of unmodeled disturbances (leader acceleration) and measurement uncertainties. Sensor data processing involves fast converging image processing algorithms onboard the follower aircraft which track the leader aircraft in the presence of background clutter and derive noisy measurements of the leader aircraft's position relative to the follower [1,2]. A consequence of using a monocular fixed camera is that range is not available as a measurement. And so the measurements from the image processing algorithm are fed into a nonlinear filter, e.g., an extended Kalman filter (EKF), which computes estimates of range and other line-of-sight (LOS) variables that are required in the guidance and control algorithms [1]. Assuming that we have useful estimates of the range and other required LOS variables, regulating these variables to desired values is not an easy problem, particularly at small ranges. In [3], an adaptive guidance algorithm and an adaptive autopilot were designed separately using a timescale separation argument, and then combined to enable the follower aircraft to maintain close range (about two wingspan lengths) from a maneuvering leader aircraft. True values of range and LOS azimuth and elevation angles were assumed, i.e., the image processing and nonlinear state filters were not implemented. Even in this case, it was found that the leader acceleration has a degrading effect on the range tracking performance. It was observed that when the leader maneuver was severe, for example a sharp heading change, the guidance algorithm of the follower would send large commands to the autopilot and cause the actuators to saturate. Consequently, the guidance commands to the autopilot were scaled down to ensure closed-loop stability for a range of leader aircraft maneuvers [3]. Scaling down the guidance commands resulted in larger overshoots from the commanded range as the severity of the leader maneuver increased. Hence performance was compromised to ensure stability.

Integrated approaches to guidance and control design have been indicated in the literature as a way to overcome the shortcomings of the timescale approach. It has been stated that an integrated guidance and control (IGC) formulation can directly compensate for the effect of autopilot lag and improve missile intercept performance [4,5]. An integrated approach also helps avoid the iterative procedure involved in tuning the guidance and autopilot subsystems, if designed separately. Integrated design is also less susceptible to saturation and stability problems. Feedback linearization of the relative cross-range and altitude to target and the roll-angle is employed in [4,5] for an IGC formulation. Sliding-mode control theory is employed in [6]. In [7], a single-plane linear IGC problem formulation is considered and a game-theoretic control synthesis approach is used. In [8], the IGC problem is formulated as a finite horizon nonlinear disturbance attenuation problem. An approximate solution approach to the preceding problem is developed which is referred to as the state-dependent Riccati differential (difference) equation (SDRDE) technique. The SDRDE technique, however, is computationally intensive owing to the need to solve Riccati difference equations online at each sample instant. An adaptive backstepping-based approach to IGC design is presented in [9]. The missile dynamics have to be written in the strict-feedback form [10] to use the backstepping approach. The advantage is that the backstepping approach can directly address plants with unmatched uncertainties. Adaptation is included to provide robustness to parametric uncertainty in the missile dynamics. In [11], the flight control system design is done via a conventional inner- and outer-loop design approach. The linear compensator gains in the inner and outer loops are chosen such that the combined error dynamics of both the loops are asymptotically stable in the absence of modeling uncertainties, and thus mitigate inner- and outer-loop interaction. Adaptation is included in both loops to address any modeling uncertainties. Pseudocontrol hedging [12] is used in the inner loop to prevent adaptation to actuator saturation and dynamics. Hedging is also used in the outer loop to prevent adaptation to inner-loop dynamics.

The main contribution of this paper is in presenting an approach to IGC design for LOS-based formation flight using a combination of adaptive output feedback inversion and backstepping techniques. No communication between the leader and follower unmanned aerial vehicles (UAVs) is assumed. This is important from both a stealth perspective and from the need to maintain autonomy of operations. The design objective is for a follower aircraft to regulate range and two bearing angle rates with respect to a maneuvering leader aircraft while maintaining turn coordination. We assume that estimates of the LOS variables are available from the use of onboard vision sensors and nonlinear filtering algorithms [1,13]. IGC design is accomplished by differentiating the LOS variables until the actuator deflection terms appear. We show the existence of a well-defined vector relative degree [14] for the multi-input/multi-output (MIMO) system of the LOS variables with respect to the actuator deflections. Then we perform approximate dynamic inversion of the LOS variable dynamics. Adaptive neural networks (NNs) are trained online with available measurements to compensate for unmodeled nonlinearities in the design process. These include uncertainties due to unknown leader aircraft acceleration, and the modeling error due to parametric uncertainties in the aircraft aerodynamic derivatives. We show that this approach to IGC design results in a deficiency in turn coordination. This leads to a second contribution in which it is shown how to modify the azimuth channel portion of the inverting design using an adaptive backstepping algorithm, similar in spirit to the approach employed in [9]. Sharma and Richards [9] were concerned only with backstepping design, and only with the dynamics in the pitch plane. Furthermore, the adaptation was only to the plant uncertainties and not to the unmodeled target acceleration. In this paper, we address the full 6 degrees-of-freedom (DOF) dynamics by marrying the concept of feedback inversion with backstepping employed only to address the portion of the dynamics wherein the inverting solution is deficient. Simulation results using a nonlinear 6 DOF simulation model are presented to illustrate the

efficacy of the approach by comparing the performance with an adaptive timescale separation-based guidance and control design.

The organization of the paper is as follows. Section II defines the LOS variable dynamics and shows existence of well-defined vector relative degree for this problem. The control design formulation is described in detail with a summary of the relevant theory. The control design presented in this section is referred to as IGC design 1. In Sec. III, the control designs for the azimuth channel and for maintaining turn coordination are modified to compensate for a deficiency in IGC design 1, which is shown to result in unacceptably large sideslip angles during turning maneuvers. The modified design in this section is referred to as IGC design 2. In Sec. IV, the results of simulation and their discussion are given. Section V presents the conclusions.

II. Integrated Guidance and Control Using Neural Networks: Design 1

This section presents an adaptive approach to IGC design for LOS-based formation flight. We formulate the problem as an adaptive output feedback control problem for a leader-follower formation flight configuration.

A. Line-of-Sight Variable Dynamics

The local north-east-down (NED) coordinate frame is assumed to be the inertial coordinate axes for the derivation of the LOS dynamics. We also assume that the NED frame is parallel to the vehicle-carried frame, which is a frame attached to the body of the follower aircraft and translating with the follower aircraft. These are reasonable assumptions in small UAV applications where the UAVs do not fly at very high altitudes or at very high (supersonic or faster) speeds. The LOS variables in the spherical coordinates consist of the range R to the leader, azimuth angle λ_A from the inertial x axis to the projection of the LOS vector onto the x–y plane, and elevation angle λ_E to the horizontal (inertial x–y plane). The LOS variables in the spherical coordinates are given in terms of the components of the LOS vector in the inertial frame as follows:

$$R = \sqrt{R_X^2 + R_Y^2 + R_Z^2} \tag{1}$$

$$\lambda_A = \tan^{-1}\left(\frac{R_Y}{R_X}\right) \tag{2}$$

$$\lambda_E = \tan^{-1}\left(\frac{-R_Z}{\sqrt{R_X^2 + R_Y^2}}\right) \tag{3}$$

The inertial frame components of the LOS vector are given in terms of the spherical coordinates as

$$R_X = R\cos\lambda_A\cos\lambda_E \tag{4}$$

$$R_Y = R\sin\lambda_A\cos\lambda_E \tag{5}$$

$$R_Z = -R\sin\lambda_E \tag{6}$$

By differentiating Eq. (1) with respect to time and using Eqs. (4–6), we can obtain the range dynamics

$$\dot{R} = \dot{R}_X\cos\lambda_A\cos\lambda_E + \dot{R}_Y\sin\lambda_A\cos\lambda_E - \dot{R}_Z\sin\lambda_E \tag{7}$$

The LOS angle dynamics are obtained by differentiating Eqs. (2) and (3) and using Eqs. (4–6)

$$\dot{\lambda}_A = \frac{1}{R\cos\lambda_E}(-\dot{R}_X\sin\lambda_A + \dot{R}_Y\cos\lambda_A) \tag{8}$$

$$\dot{\lambda}_E = -\frac{1}{R}(\dot{R}_X\cos\lambda_A\sin\lambda_E + \dot{R}_Y\sin\lambda_A\sin\lambda_E + \dot{R}_Z\cos\lambda_E) \tag{9}$$

where $\dot{R}_X$, $\dot{R}_Y$, $\dot{R}_Z$ denote the relative velocity components between the leader and follower aircraft expressed in the inertial coordinate system, which are related to range rate and LOS rate as follows:

$$\dot{R}_X = \dot{R}\cos\lambda_A\cos\lambda_E - R\dot{\lambda}_A\sin\lambda_A\cos\lambda_E - R\dot{\lambda}_E\cos\lambda_A\sin\lambda_E \tag{10}$$

$$\dot{R}_Y = \dot{R}\sin\lambda_A\cos\lambda_E + R\dot{\lambda}_A\cos\lambda_A\cos\lambda_E - R\dot{\lambda}_E\sin\lambda_A\sin\lambda_E \tag{11}$$

$$\dot{R}_Z = -\dot{R}\sin\lambda_E - R\dot{\lambda}_E\cos\lambda_E \tag{12}$$

By differentiating Eqs. (7–9) and using Eqs. (10–12), we obtain the following relation between the relative accelerations and the second time derivatives of the range and LOS angles:

$$\ddot{R} = R[\dot{\lambda}_A^2\cos^2\lambda_E + \dot{\lambda}_E^2] + [a_{X_I}\cos\lambda_A\cos\lambda_E + a_{Y_I}\sin\lambda_A\cos\lambda_E - a_{Z_I}\sin\lambda_E] \tag{13}$$

$$\ddot{\lambda}_A = \frac{1}{\cos\lambda_E}\left\{-2\dot{\lambda}_A\left[\left(\frac{\dot{R}}{R}\right)\cos\lambda_E - \dot{\lambda}_E\sin\lambda_E\right] + \left(\frac{1}{R}\right)[-a_{X_I}\sin\lambda_A + a_{Y_I}\cos\lambda_A]\right\} \tag{14}$$

$$\ddot{\lambda}_E = -2\left(\frac{\dot{R}}{R}\right)\dot{\lambda}_E - \dot{\lambda}_A^2\sin\lambda_E\cos\lambda_E - \left(\frac{1}{R}\right)[a_{X_I}\cos\lambda_A\sin\lambda_E + a_{Y_I}\sin\lambda_A\sin\lambda_E + a_{Z_I}\cos\lambda_E] \tag{15}$$

where $a_{X_I} = a_{L_{X,I}} - a_{F_{X,I}} \equiv \ddot{R}_X$, $a_{Y_I} = a_{L_{Y,I}} - a_{F_{Y,I}} \equiv \ddot{R}_Y$, $a_{Z_I} = a_{L_{Z,I}} - a_{F_{Z,I}} \equiv \ddot{R}_Z$ are the relative accelerations of the leader with respect to the follower in the inertial plane. Subscripts 'L' and 'F' denote leader and follower aircraft, respectively.

B. Control Formulation

The standard form of the equations of motion used for describing formation flight can be written as

$$\dot{\bar{x}} = f(\bar{x}, \bar{a}_L) + \sum_{i=1}^{4} g_i(\bar{x})u_i \quad \text{and} \quad \bar{y} = h(\bar{x}) \tag{16}$$

where the state vector $\bar{x} = [U\ V\ W\ p\ q\ r\ \Phi\ \Theta\ \Psi\ R\ \lambda_A\ \lambda_E\ \dot{R}\ \dot{\lambda}_A\ \dot{\lambda}_E]^T$, the input vector $\bar{u} = [\delta T\ \delta a\ \delta e\ \delta r]^T$, $\bar{u}(t) \in R^4$, the output vector $\bar{y} = [R, \dot{\lambda}_A - \dot{\Psi}, \dot{\lambda}_E - \dot{\Theta}, \Phi]^T$, $\bar{y}(t) \in R^4$, and the leader motion state vector $\bar{a}_L = [a_{L_{X_I}}, a_{L_{Y_I}}, a_{L_{Z_I}}]^T$.

The objective of the control law design is for the follower aircraft to maintain a prescribed range to the leader aircraft in the presence of leader maneuvers and other unmodeled disturbances. In the formulation, the output variables to be regulated are chosen as $[R, \dot{\lambda}_A - \dot{\Psi}, \dot{\lambda}_E - \dot{\Theta}, \Phi]^T$. The bank angle Φ command is constructed to maintain turn coordination, that is, to nullify the side acceleration along the y axis of the body-fixed frame. The range command is given by a constant value, which is chosen as the length of two wingspans in the examples that follow. The variables $\chi_A \equiv \lambda_A - \Psi$ and $\chi_E \equiv \lambda_E - \Theta$ represent the bearing angles in the NED frame. These angles are computable from the body attitude and LOS measurements obtained from an onboard camera fixed to the body of the follower aircraft, with the optical axis of the camera coincident with the body x axis. The bearing angle rate commands are set to zero. The bearing angles are not regulated because it is not desirable

to restrict the follower aircraft to a particular orientation with respect to the leader aircraft, particularly in the presence of leader maneuvers.

1. Vector Relative Degree and Approximate Feedback Linearization

To show the existence of a well-defined vector relative degree, the output variables are differentiated until the control variables appear. The first step in this direction is to transform the follower acceleration terms $\{a_{F_{X,I}}, a_{F_{Y,I}}, a_{F_{Z,I}}\}$, in Eqs. (13–15) in the inertial frame, into the follower body-axes coordinate frame. It is also preferred to use the specific force vector in the body-axes coordinate frame instead of the acceleration vector, because the specific force vector is a directly measured quantity. This is accomplished by first subtracting the gravity vector

$$\begin{bmatrix} a_{F_{X,B}} \\ a_{F_{Y,B}} \\ a_{F_{Z,B}} \end{bmatrix} = [L_x(\Phi)][L_y(\Theta)][L_z(\Psi)] \cdot \left(\begin{bmatrix} a_{F_{X,I}} \\ a_{F_{Y,I}} \\ a_{F_{Z,I}} \end{bmatrix} - \begin{bmatrix} 0 \\ 0 \\ g \end{bmatrix} \right) \tag{17}$$

which implies

$$\begin{bmatrix} a_{F_{X,I}} \\ a_{F_{Y,I}} \\ a_{F_{Z,I}} \end{bmatrix} = [L_z(-\Psi)][L_y(-\Theta)][L_x(-\Phi)] \begin{bmatrix} a_{F_{X,B}} \\ a_{F_{Y,B}} \\ a_{F_{Z,B}} \end{bmatrix} + \begin{bmatrix} 0 \\ 0 \\ g \end{bmatrix} \tag{18}$$

In Eqs. (17) and (18), the variable $[L]$ represents a rotation matrix and the subscript indicates the axis about which the rotation occurs. The terms $\{a_{F_{X,B}}, a_{F_{Y,B}}, a_{F_{Z,B}}\}$ are measurable acceleration components in the body-fixed coordinates and will be used in feedback loop in the controller. It is assumed that only the X component of $\{a_{F_{X,B}}, a_{F_{Y,B}}, a_{F_{Z,B}}\}$ has a functional relation to the throttle among the control input variables $\{\delta T, \delta a, \delta e, \delta r\}$ of the follower aircraft. The Y and Z components are assumed to be independent of the control input variables because their dependency is secondary. Thus

$$a_{F_{X,B}} = a_{F_{X,B0}} + \Delta a_{F_{X,B}} \tag{19}$$

where $a_{F_{X,B0}} = (\Im_{A_{X,0}} + \Im_{T_{X,0}})/m$, $\Delta a_{F_{X,B}} = (\Delta\Im_{A_X} + \Delta\Im_{T_X})/m = \cdots + X_{\delta T} \cdot \delta T$, where $\Im$ refers to the external force acting on the aircraft, and the variables $\Im_A$, $\Im_T$ refer to the external force due to aerodynamics and thrust, respectively. Combining Eqs. (18) and (19) into Eqs. (13–15), we obtain

$$\begin{bmatrix} \ddot{R} \\ \ddot{\lambda}_A \\ \ddot{\lambda}_E \end{bmatrix} = \begin{bmatrix} \Delta_R(\bar{x}, \bar{a}_L) \\ \Delta_{\lambda_A}(\bar{x}, \bar{a}_L) \\ \Delta_{\lambda_E}(\bar{x}, \bar{a}_L) \end{bmatrix} + \begin{bmatrix} -\cos(\Psi - \lambda_A)\cos\lambda_E \cos\Theta - \sin\lambda_E \sin\Theta \\ -\sin(\Psi - \lambda_A)\cos\Theta/(R\cos\lambda_E) \\ [\cos(\Psi - \lambda_A)\sin\lambda_E \cos\Theta - \cos\lambda_E \sin\Theta]/R \end{bmatrix} X_{\delta T}\delta T \tag{20}$$

where the vector $[\Delta_R, \Delta_{\lambda_A}, \Delta_{\lambda_E}]^T$ is a function of the LOS variables, the leader acceleration terms, and the follower aircraft motion variables.

The next step is to obtain the time derivatives of the Euler angles Ψ, Θ, and Φ in terms of the remaining control effectors. To do this, first consider the relationship between the Euler angle rates and the angular velocities [15]

$$\begin{gathered} \dot{\Phi} = p + (q\sin\Phi + r\cos\Phi)\tan\Theta \qquad \dot{\Theta} = q\cos\Phi - r\sin\Phi \\ \dot{\Psi} = (q\sin\Phi + r\cos\Phi)\sec\Theta \end{gathered} \tag{21}$$

and thus the second time derivatives of Euler angles $\{\Phi, \Theta, \Psi\}$ can be expressed in the form

$$\begin{aligned} \ddot{\Phi} &= \dot{p} + (\dot{q}\sin\Phi + \dot{r}\cos\Phi)\tan\Theta + f_\Phi(\bar{x}) \\ \ddot{\Theta} &= \dot{q}\cos\Phi - \dot{r}\sin\Phi + f_\Theta(\bar{x}) \\ \ddot{\Psi} &= (\dot{q}\sin\Phi + \dot{r}\cos\Phi)\sec\Theta + f_\Psi(\bar{x}) \end{aligned} \tag{22}$$

where $\{f_\Phi(\bar{x}), f_\Theta(\bar{x}), f_\Psi(\bar{x})\}$ are computable functions of the angular velocities and Euler angles. The derivatives of the angular velocities $\{\dot{p}, \dot{q}, \dot{r}\}$ depend mainly on the control surface perturbations $\{\delta a, \delta e, \delta r\}$,

$$\dot{p} = \Delta_p^1(\bar{x}) + L_{\delta a}\cdot\delta a \quad \dot{q} = \Delta_q^1(\bar{x}) + M_{\delta e}\cdot\delta e \quad \dot{r} = \Delta_r^1(\bar{x}) + N_{\delta r}\cdot\delta r \tag{23}$$

where $\{\Delta_p^1, \Delta_q^1, \Delta_r^1\}$ are functions of the states of the aircraft dynamics. Using Eq. (23) in Eq. (22), we obtain

$$\begin{aligned} \ddot{\Phi} &= \Delta_\Phi(\bar{x}) + L_{\delta a}\cdot\delta a + M_{\delta e}\sin\Phi\tan\Theta\cdot\delta e \\ &\quad + N_{\delta r}\cos\Phi\tan\Theta\cdot\delta r \\ \ddot{\Theta} &= \Delta_\Theta(\bar{x}) + M_{\delta e}\cos\Phi\cdot\delta e - N_{\delta r}\sin\Phi\cdot\delta r \\ \ddot{\Psi} &= \Delta_\Psi(\bar{x}) + M_{\delta e}\sin\Phi\sec\Theta\cdot\delta e + N_{\delta r}\cos\Phi\sec\Theta\cdot\delta r \end{aligned} \tag{24}$$

Thus, we have the following relations

$$\begin{bmatrix} \ddot{R} \\ \ddot{\lambda}_A - \ddot{\Psi} \\ \ddot{\lambda}_E - \ddot{\Theta} \\ \ddot{\Phi} \end{bmatrix} = [\bar{\boldsymbol{\Delta}}(\bar{x}, \bar{a}_L)] + [A(\bar{x})] \begin{bmatrix} \delta T \\ \delta a \\ \delta e \\ \delta r \end{bmatrix} \tag{25}$$

where

$$A(\bar{x}) = \begin{bmatrix} -X_{\delta T}\{\cos(\Psi - \lambda_A)\cos\lambda_E\cos\Theta + \sin\lambda_E\sin\Theta\} & 0 & 0 & 0 \\ -X_{\delta T}\sin(\Psi - \lambda_A)\cos\Theta/R\cos\lambda_E & 0 & -M_{\delta e}\sin\Phi\sec\Theta & -N_{\delta r}\cos\Phi\sec\Theta \\ X_{\delta T}\{\cos(\Psi - \lambda_A)\sin\lambda_E\cos\Theta - \cos\lambda_E\sin\Theta\}/R & 0 & -M_{\delta e}\cos\Phi & N_{\delta r}\sin\Phi \\ 0 & L_{\delta a} & M_{\delta e}\sin\Phi\tan\Theta & N_{\delta r}\cos\Phi\tan\Theta \end{bmatrix} \tag{26}$$

A well-defined vector relative degree [14] exists if and only if $A(\bar{x})$ is nonsingular. Its determinant is given by

$$\det A(\bar{x}) = X_{\delta T}L_{\delta a}M_{\delta e}N_{\delta r}\{\cos(\Psi - \lambda_A)\cos\lambda_E + \sin\lambda_E\tan\Theta\} \tag{27}$$

Because we regulate range, bank angle, and the bearing rates, the system has a well-defined vector relative degree $\{2, 1, 1, 2\}$ unless the quantity in braces is zero. The term in the parentheses is the (1, 1) th element of the $A(\bar{x})$ matrix multiplied by $\sec\Theta$. And so, $\det A(\bar{x}) = 0$ implies that the range is not controllable using the throttle δT. Geometrically, this happens when:

1) $\chi_A = \pi/2$ and $\lambda_E = 0$ *or* $\chi_A = \pi/2$ and $\Theta = 0$. This condition implies that the follower heading is perpendicular to the LOS when the motion is in the horizontal plane.

2) $\lambda_E = \pm\pi/2$ and $\Theta = 0$ assuming $|\Theta| < \pi/2$. This condition implies that the follower is either directly above or below the leader aircraft.

To minimize the likelihood of these situations arising, we impose soft limits on the azimuth and elevation bearing angles $|\chi_A| \leq \chi_{A_{\max}} < \pi/2$ and $|\chi_E| \leq \chi_{E_{\max}} < \pi/2$ in our problem formulation. This is enabled by adjusting the bearing rate commands to prevent drifts in the bearing angles to values greater than maximum field-of-view widths. This is mentioned in Sec. IV.B. In our implementation, we set $\chi_{A_{\max}} = \chi_{A_{\max}} = \pi/6$. We also assume the initial conditions for the bearing angles satisfy these restrictions.

The important issue is that should the vector relative degree not exist at some point in time, the condition is only temporary, and an alternative strategy can be pursued when close to this condition. For example, for LOS conditions close to the preceding two cases, we can give up on regulating range temporarily and an alternative feedback inversion control can be designed. The more serious issue is if there are any equilibrium conditions for which the vector relative degree does not exist. We have shown that by restricting the bearing angles to be less than 90 deg, we have eliminated such equilibrium conditions. In general, we can show that $\det A(\bar{\boldsymbol{x}}) \neq 0$ subject to the constraints $|\Theta| < \pi/2$, $|\chi_A| \leq \pi/4$, and $|\chi_E| \leq \pi/4$ numerically.

The process of dynamic inversion ignores the nonlinearities and leader's acceleration terms in Eq. (24). Thus an approximate feedback linearization is given as follows:

$$\begin{bmatrix} \delta T \\ \delta a \\ \delta e \\ \delta r \end{bmatrix} = [A(\bar{\boldsymbol{x}})]^{-1} \begin{bmatrix} \nu_R \\ \nu_{\dot{\chi}_A} \\ \nu_{\dot{\chi}_E} \\ \nu_\Phi \end{bmatrix} \tag{28}$$

where the vector $\bar{\boldsymbol{\nu}} = [\nu_R \;\; \nu_{\dot{\chi}_A} \;\; \nu_{\dot{\chi}_E} \;\; \nu_\Phi]^T$ represents the *pseudocontrol* input vector and represents the desired dynamics of the output vector $[R, \dot{\lambda}_A - \dot{\Psi}, \dot{\lambda}_E - \dot{\Theta}, \Phi]^T$. Thus the system dynamics, as far as the regulated output variables are concerned, from Eq. (25) and (28), are given by

$$\bar{\boldsymbol{y}}^{(r)} = \bar{\boldsymbol{\Delta}} + \bar{\boldsymbol{\nu}}$$

where $\bar{\boldsymbol{y}}^{(r)} = [\ddot{R} \;\; \ddot{\lambda}_A - \ddot{\Psi} \;\; \ddot{\lambda}_E - \ddot{\Theta} \;\; \ddot{\Phi}]^T$, where $r = \{2, 1, 1, 2\}$ is the vector relative degree and $\bar{\boldsymbol{\Delta}} = \bar{\boldsymbol{\Delta}}(\bar{\boldsymbol{x}}, \bar{\boldsymbol{a}}_L)$ is the modeling error vector consisting of the LOS variables, leader acceleration terms, and follower aircraft motion variables.

The bank angle command is constructed to maintain turn coordination, that is, to nullify the side acceleration along the y axis of the body-fixed frame. This can be accomplished in several ways. One such way is to use a proportional-derivative controller to generate the bank angle command to regulate the side acceleration to zero.

2. *Controller Design Using Adaptive Output Feedback*

The objective of the control design is for the output vector $\bar{\boldsymbol{y}} = [R \;\; \dot{\lambda}_A - \dot{\Psi} \;\; \dot{\lambda}_E - \dot{\Theta} \;\; \Phi]^T$ to track a stable, bounded reference trajectory vector $\bar{\boldsymbol{y}}_c$. The pseudocontrol is chosen to have the form [16,17]

$$\bar{\boldsymbol{\nu}} = \bar{\boldsymbol{y}}_c^{(r)} + \bar{\boldsymbol{\nu}}_{\text{dc}} - \bar{\boldsymbol{\nu}}_{\text{ad}} \tag{29}$$

where $\bar{\boldsymbol{y}}_c^{(r)}$, the rth derivatives of the reference trajectory vector $\bar{\boldsymbol{y}}_c$, are generated by stable reference models that define the desired closed-loop behavior, $\bar{\boldsymbol{\nu}}_{\text{dc}}$ is the vector output of linear dynamic compensators designed to stabilize the linearized error dynamics, and $\bar{\boldsymbol{\nu}}_{\text{ad}}$ is the vector adaptive component designed to cancel the effect of the modeling error vector $\bar{\boldsymbol{\Delta}}$.

Because range has relative degree 2, the plant transfer function from the pseudocontrol ν_R to R is $1/s^2$. A first-order lead-lag compensator structure was selected to stabilize the range error dynamics according to the direct adaptive output feedback approach of [16]. In addition, the pole-placement approach was used to satisfy a strictly positive real (SPR) condition. The resulting two outputs of the compensator are given by

$$\begin{bmatrix} \nu_{\text{dc},R} \\ \tilde{y}_{\text{ad},R} \end{bmatrix} = \frac{1}{s+7} \begin{bmatrix} 8(s+1) \\ 20(s+1) \end{bmatrix} \cdot \tilde{y}_R(s) \tag{30}$$

which places the closed-loop poles of the error dynamics at -3, $-1 \pm j$. A sigma-pi (SP) NN with 47 neurons was used as the adaptive element. The variables $[1, \bar{x}^T, \nu_R, \tilde{y}_{\text{ad},R}]^T$ were used as inputs to the NN. All the NN inputs were normalized using an estimate for their maximum values. The NN gains were set to $F_R = 50$ and $\lambda_{W,R} = 1$. Range was commanded to follow the output of a second-order reference model, designed with a natural frequency of $\omega_{n_R} = 1$ rad/s and damping $\varsigma_R = 0.8$.

Because the bearing angle rates $\dot{\chi}_A$ and $\dot{\chi}_E$ are relative degree 1 outputs, the linear compensators corresponding to these outputs are just proportional error controllers. The gains of the proportional error controller were chosen as $K_{\dot{\chi}_A} = 10$ and $K_{\dot{\chi}_E} = 10$. Thus their designs follow a state feedback approach, and the tracking error of the bearing angles rates are directly used as training signals for the NN:

$$\begin{bmatrix} \nu_{\text{dc},\dot{\chi}_A} \\ \tilde{y}_{\text{ad},\dot{\chi}_A} \end{bmatrix} = \begin{bmatrix} K_{\dot{\chi}_A} \tilde{y}_{\dot{\chi}_A} \\ \tilde{y}_{\dot{\chi}_A} \end{bmatrix} \tag{31}$$

$$\begin{bmatrix} \nu_{\text{dc},\dot{\chi}_E} \\ \tilde{y}_{\text{ad},\dot{\chi}_E} \end{bmatrix} = \begin{bmatrix} K_{\dot{\chi}_E} \tilde{y}_{\dot{\chi}_E} \\ \tilde{y}_{\dot{\chi}_E} \end{bmatrix} \tag{32}$$

The command filters are chosen as first-order systems with time constants of $\tau_{\dot{\chi}_A} = \tau_{\dot{\chi}_E} = 1$. The NN used in each channel has the same form as in the range channel except with the input vectors given by $[1, \bar{\boldsymbol{x}}^T, \nu_{\dot{\chi}_A}, \tilde{y}_{\dot{\chi}_A}]^T$ and $[1, \bar{\boldsymbol{x}}^T, \nu_{\dot{\chi}_E}, \tilde{y}_{\dot{\chi}_E}]^T$, respectively, and the network gains of $F_{\dot{\chi}_A} = 100$, $\lambda_{W,\dot{\chi}_A} = 0.5$, and $F_{\dot{\chi}_E} = 100$, $\lambda_{W,\dot{\chi}_E} = 0.5$.

The bank angle command Φ_{com} for maintaining turn coordination is filtered through a second-order command filter to generate the reference bank angle command Φ_c. Because the bank angle has relative degree 2, a first-order lead-lag compensator structure was selected to stabilize the bank angle error dynamics. By using pole-placement to satisfy the SPR condition, the resulting two outputs of the compensator are given by

$$\begin{bmatrix} \nu_{\text{dc},\Phi} \\ \tilde{y}_{\text{ad},\Phi} \end{bmatrix} = \frac{1}{s+10} \begin{bmatrix} 8(s+1) \\ 20(s+1) \end{bmatrix} \cdot \tilde{y}_\Phi(s) \tag{33}$$

which places the closed-loop poles of the error dynamics at -3, $-1 \pm j$. The variables $[1, \bar{\boldsymbol{x}}^T, \nu_\Phi, \tilde{y}_{\text{ad},\Phi}]^T$ were used as inputs to the NN. All of the NN inputs were normalized using an estimate for their maximum values. The network gains were $F_\Phi = 100$ and $\lambda_{W,\Phi} = 1$. The bank angle was commanded to follow the output of a second-order reference model, designed with a natural frequency of $\omega_{n_\Phi} = 5$ rad/s and damping $\varsigma_\Phi = 0.8$.

The NN adaptation rule for each channel is given from the extensions of Lyapunov theory [18]

$$\dot{\hat{W}} = -F(\tilde{y}_{\text{ad}} \boldsymbol{\phi}_f + \lambda_W \hat{W}) \tag{34}$$

where $F > 0$ and $\lambda_W > 0$ are the adaptation gains, and $\boldsymbol{\phi}_f$ is the filtered basis function vector of the NN. Figure 1 shows a block diagram implementation of the controller design.

3. *Pseudocontrol Hedging*

Any dynamics and nonlinearities associated with actuators have not yet been considered in the design. If the actuators become position or rate saturated, the reference models will continue to demand tracking as though full authority were still available. Furthermore, when an adaptive element such as a neural network is introduced, these actuator nonlinearities will appear in the tracking error dynamics resulting in the adaptive element attempting to correct for them. Pseudocontrol hedging (PCH) is introduced to protect the adaptive law from effects due to actuator rate and position limits, unmodeled actuator dynamics, and to protect the adaptive

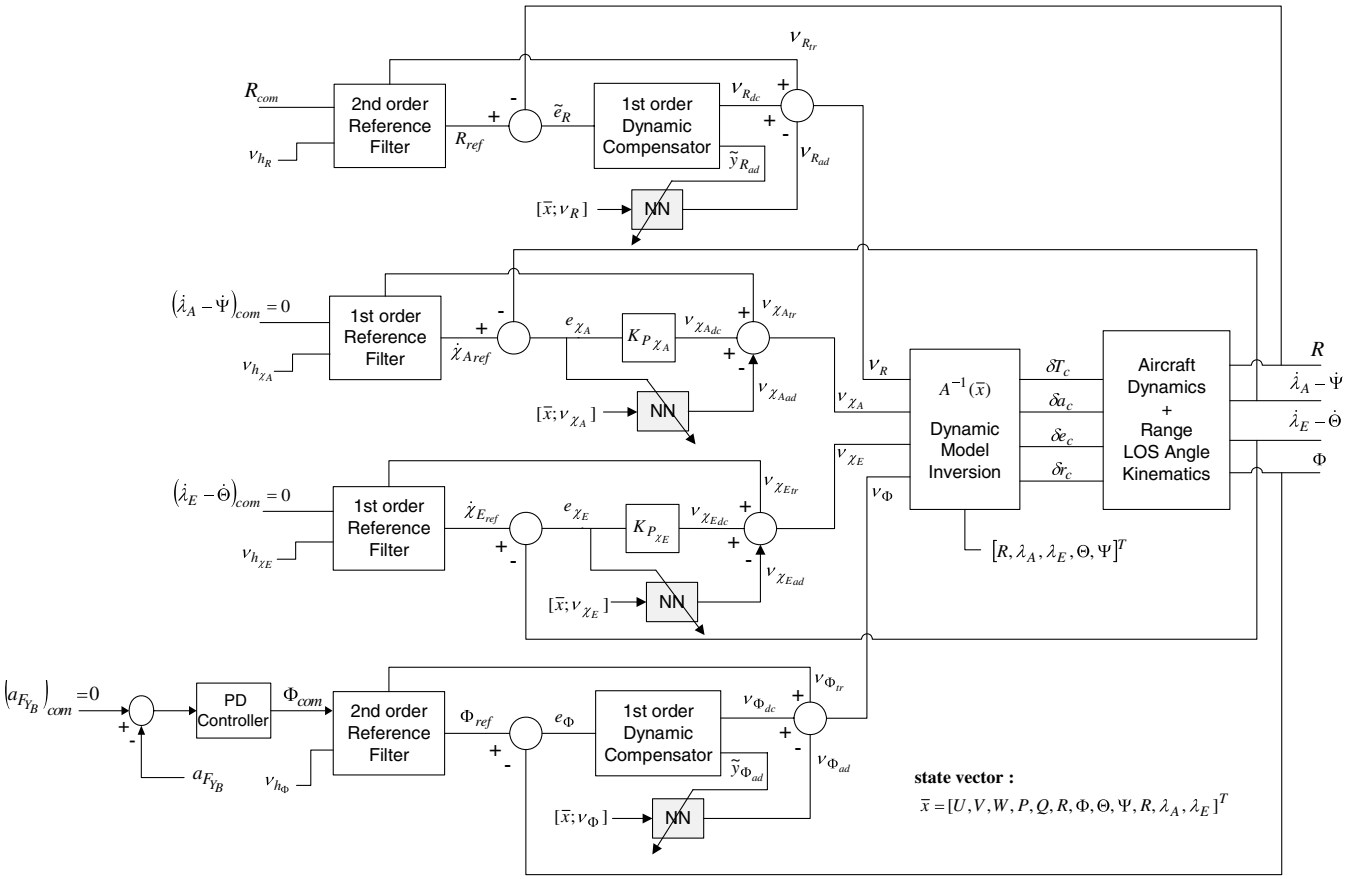

Fig. 1 Integrated guidance and control logic block diagram for follower aircraft: design 1.

process when it is not in control of the plant. The main idea behind PCH methodology is to modify the reference command to prevent the adaptive element from adapting to these actuator characteristics, while allowing adaptation to other effects to continue. This is commonly done by generating the command using a reference model for the desired response. The reference model is "hedged" by an amount equal to the difference between the commanded and an estimate for the achieved pseudocontrol [12].

4. Remark

The IGC design developed earlier leads to unacceptably large sideslip angles, as will be shown in the simulation results. The problem here can be noticed by examining the first three rows of Eq. (25) and the matrix $A(\bar{\boldsymbol{x}})$ in Eq. (26). It can be seen that the derivatives $\ddot{R}$, $\ddot{\lambda}_A - \ddot{\Psi}$, and $\ddot{\lambda}_E - \ddot{\Theta}$ do not contain the aileron deflection term δa. Specifically, the term $\ddot{\lambda}_A - \ddot{\Psi}$, which is the second derivative of the azimuth bearing angle $\lambda_A - \Psi$, shows strong dependence on the rudder deflection δr for small bank angle Φ. This implies that the rudder is used to generate a heading rate to regulate the azimuth bearing rate to zero. Using the rudder in this way causes uncoordinated turns leading to unacceptably large sideslip angles. In the next section, the azimuth channel is redesigned using the approach of adaptive backstepping [9,10] to avoid using the rudder to control the azimuth rate.

III. Integrated Guidance and Control Using Neural Networks: Design 2

We worked extensively with the IGC-1 design for reducing the large sideslip excursions. After many weeks of trying everything of which we could think, we finally abandoned it in favor of a backstepping approach to redesign the azimuth channel. The idea behind the redesign of the azimuth channel is to show that there exists a natural dependency of the azimuth rate derivative $\ddot{\lambda}_A$ on the bank angle Φ, and consequently on the aileron deflection δa. Then this natural dependency can be exploited in a strategy to implement adaptive backstepping in terms of three feedback loops as follows:

$$(\dot{\lambda}_A) \rightarrow (\Phi) \rightarrow (p) \rightarrow (\delta a)$$

A. Azimuth Rate Control via Backstepping Design

The first step is to rewrite Eq. (14) as follows

$$\begin{aligned}\ddot{\lambda}_A = {} & \frac{-2\dot{\lambda}_A}{\cos\lambda_E}\left[\left(\frac{\dot{R}}{R}\right)\cos\lambda_E - \dot{\lambda}_E \sin\lambda_E\right] \\ & + \left(\frac{1}{R\cos\lambda_E}\right)[-a_{L_{X_I}}\sin\lambda_A + a_{L_{Y_I}}\cos\lambda_A \\ & - (-a_{F_{X_I}}\sin\lambda_A + a_{F_{Y_I}}\cos\lambda_A)] \end{aligned} \tag{35}$$

where $a_{F_{X_I}}$ and $a_{F_{Y_I}}$ represent the x- and y-axis acceleration components of follower aircraft expressed in the Cartesian inertial coordinates, respectively. Then the following equality can be derived

$$\begin{aligned} & -a_{F_{X_I}}\sin\lambda_A + a_{F_{Y_I}}\cos\lambda_A \\ & \quad = -a_{F_{X_1}}\sin(\lambda_A - \Psi) + a_{F_{Y_1}}\cos(\lambda_A - \Psi) \end{aligned} \tag{36}$$

where $a_{F_{X_1}}$ and $a_{F_{Y_1}}$ represent the x- and y-axis acceleration components of follower aircraft expressed in the coordinate frame obtained by a rotation about the inertial z axis by the Euler angle Ψ.

From the pictorial representation of the coordinate frames in the inertial horizontal plane in Fig. 2, $a_{F_{Y_1}}$ can be approximated as follows

$$a_{F_{Y_1}} \approx V_F \cos\Theta \cdot \dot{\Psi}_{F_W} \approx V_F \cos\Theta(\dot{\Psi} + \dot{\beta}) \tag{37}$$

where the subscript 'W' indicates the wind axes. Then the following

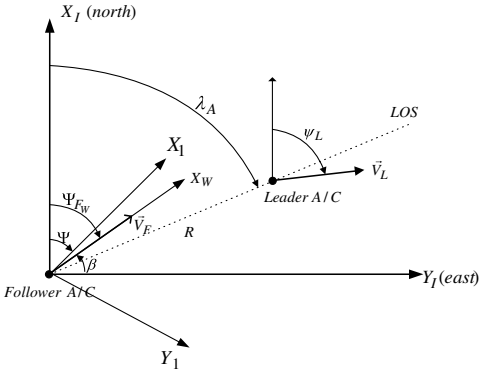

Fig. 2 Coordinate reference frames in horizontal plane.

identities can be used to expand Eq. (37)

$$\dot{\Psi} = (q \sin \Phi + r \cos \Phi) \sec \Theta \tag{38}$$

$$\begin{aligned}\dot{\beta} &= p \sin\alpha - r\cos\alpha + \frac{1}{mV_F}(D\sin\beta + Y\cos\beta)\\ &+ \frac{g}{V_F}(\cos\alpha\sin\beta\sin\Theta + \cos\beta\sin\Phi\cos\theta\\ &- \sin\alpha\sin\beta\cos\Phi\cos\Theta)\end{aligned} \tag{39}$$

Equation (35) can be rewritten as follows by using Eqs. (36–39)

$$\ddot{\lambda}_A = f_1(\bar{x}) + g_1(\bar{x}) \cdot \Phi + \Delta^2_{\lambda_A}(\bar{x}, \bar{a}_L) \tag{40}$$

where

$$\begin{aligned}f_1(\bar{x}) &= \frac{-2\dot{\lambda}_A}{\cos\lambda_E}\left[\left(\frac{\dot{R}}{R}\right)\cos\lambda_E - \dot{\lambda}_E \sin\lambda_E\right]\\ &+ \left(\frac{1}{R\cos\lambda_E}\right)a_{F_{X,1}}\sin(\lambda_A - \Psi)\\ g_1(\bar{x}) &= -\frac{\cos(\lambda_A - \Psi)}{R\cos\lambda_E}(V_F q + g\cos\beta\cos^2\Theta)\end{aligned} \tag{41}$$

are known, computable terms, and $\Delta^2_{\lambda_A}(\bar{x}, \bar{a}_L)$ is the modeling error due to ignored terms in the $\ddot{\lambda}_A$ dynamics, which is different from $\Delta_{\lambda_A}(\bar{x}, \bar{a}_L)$ in Eq. (20). We also have

$$\begin{gathered}\dot{\Phi} = f_2(\bar{x}) + g_2 p, \qquad f_2(\bar{x}) = (q\sin\Phi + r\cos\Phi)\tan\Theta\\ g_2 = 1\end{gathered} \tag{42}$$

$$\begin{gathered}\dot{p} = f_3(\bar{x}) + g_3\delta a + \Delta^2_p(\bar{x}, \delta a), \quad f_3(\bar{x}) = L_v v + L_p p + L_r r\\ g_3 = L_{\delta a}\end{gathered} \tag{43}$$

where $f_2(\bar{x})$, $f_3(\bar{x})$, g_2, g_3 are known, computable terms, and $\Delta^2_p(\bar{x}, \delta a)$ is the modeling error due to ignored terms in the roll-rate dynamics, which is different from $\Delta^1_p(\bar{x})$ in Eq. (23). Equations (40–43) show that the azimuth rate dynamics have a natural cascade form. That is, Φ can be used as a virtual control for the $\dot{\lambda}_A$ dynamics, and p as a virtual control for the Φ dynamics, with the control δa finally being computed to ensure $\dot{\lambda}_A$ command tracking. Let $x_1 \equiv \dot{\lambda}_A$, $x_2 \equiv \Phi$, $x_3 \equiv p$, and $u \equiv \delta a$. Then Eqs. (40–43) can be rewritten as follows:

$$\dot{x}_1 = f_1(\bar{x}) + g_1(\bar{x})x_2 + \Delta^2_{\lambda_A}(\bar{x}, \bar{a}_L) \tag{44}$$

$$\dot{x}_2 = f_2(\bar{x}, x_2) + x_3 \tag{45}$$

$$\dot{x}_3 = f_3(\bar{x}, x_3) + g_3 u + \Delta^2_p(\bar{x}, \delta a) \tag{46}$$

With the plant dynamics cast in the proper form, an adaptive backstepping method is presented. We begin by defining the following error states

$$\zeta_1 \equiv x_{1c} - x_1 \tag{47}$$

$$\zeta_2 \equiv g_1 \cdot (x_{2,\text{com}} - x_2) \tag{48}$$

$$\zeta_3 \equiv g_1 \cdot (x_{3,\text{com}} - x_3) \tag{49}$$

where $x_{2,\text{com}}$ and $x_{3,\text{com}}$ are virtual commands to be constructed that will ensure that the command x_{1c} is tracked. The reference command x_{1c} is obtained by filtering the raw azimuth bearing rate command through a stable command filter that generates smooth, achievable trajectories.

Step 1: Differentiating ζ_1 of Eq. (47) and applying Eqs. (44) and (48) yields

$$\begin{aligned}\dot{\zeta}_1 &= \dot{x}_{1c} - \dot{x}_1 = \dot{x}_{1c} - f_1 - g_1 x_2 - \Delta^2_{\lambda_A}\\ &= \dot{x}_{1c} - f_1 + \zeta_2 - g_1 x_{2,\text{com}} - \Delta^2_{\lambda_A}\end{aligned} \tag{50}$$

where $x_{2,\text{com}}$ is viewed as a virtual control for the ζ_1 dynamics. Then to stabilize Eq. (50), let

$$x_{2,\text{com}} = g_1^{-1}[K_1\zeta_1 - f_1 + \dot{x}_{1c} - u_{\text{ad},1}] \tag{51}$$

where $u_{\text{ad},1}$ is an adaptive control term designed to cancel $\Delta^2_{\lambda_A}$ and $|\psi - \lambda_A| < \pi/2$ for g_1 to be invertible. Then substituting Eq. (51) into Eq. (50) yields

$$\dot{\zeta}_1 = -K_1\zeta_1 + \zeta_2 + u_{\text{ad},1} - \Lambda_1 \tag{52}$$

where $\Lambda_1 = \Delta^2_{\lambda_A}$. In ideal conditions, $u_{\text{ad},1} = \Lambda_1$ and $x_2 \to x_{2,\text{com}}$, so that the error $\zeta_2 \to 0$, and the ζ_1 dynamics become asymptotically stable.

Step 2: Differentiating ζ_2 yields

$$\begin{aligned}\dot{\zeta}_2 &= \dot{g}_1(x_{2,\text{com}} - x_2) + g_1(\dot{x}_{2,\text{com}} - \dot{x}_2) = \dot{g}_1(x_{2,\text{com}} - x_2)\\ &+ g_1\dot{x}_{2,\text{com}} - g_1\dot{x}_2 = -\Lambda_2 + \ddot{x}_{1c} - g_1 x_3 - g_1 f_2\\ &= -\Lambda_2 + \ddot{x}_{1c} - g_1 f_2 + \zeta_3 - g_1 x_{3,\text{com}}\end{aligned} \tag{53}$$

where $\Lambda_2 \equiv -[\dot{g}_1(x_{2,\text{com}} - x_2) + g_1\dot{x}_{2,\text{com}} - \ddot{x}_{1c}]$ because the derivatives of f_1 and g_1 contain unknown terms due to leader aircraft motion. Let

$$x_{3,\text{com}} = g_1^{-1}[\zeta_1 + K_2\zeta_2 + \ddot{x}_{1c} - g_1 f_2 - u_{\text{ad},2}] \tag{54}$$

so that

$$\dot{\zeta}_2 = -\zeta_1 - K_2\zeta_2 + \zeta_3 + u_{\text{ad},2} - \Lambda_2 \tag{55}$$

The purpose of introducing ζ_1 in Eq. (55) is to compensate for the coupling between the ζ_1 and ζ_2 dynamics. The sign of the ζ_1 in Eq. (54) is intentionally chosen as negative to set up a skew-symmetric matrix representing the complete error dynamics. This skew-symmetric structure is a key feature of backstepping controllers, and results in the cancellation of the coupling terms during Lyapunov stability analysis [10].

Step 3: This last step is very similar to the previous ones except that rather than the virtual control, the actual control signal is constructed. Differentiating ζ_3 yields

$$\begin{aligned}\dot{\zeta}_3 &= \dot{g}_1(x_{3,\text{com}} - x_3) + g_1(\dot{x}_{3,\text{com}} - \dot{x}_3) = \dot{g}_1(x_{3,\text{com}} - x_3)\\ &+ g_1\dot{x}_{3,\text{com}} - g_1\dot{x}_3 = \dot{g}_1(x_{3,\text{com}} - x_3) + g_1\dot{x}_{3,\text{com}}\\ &- g_1(f_3 + g_3 u + \Delta^2_p) = -\Lambda_3 + \ddot{x}_{1c} - g_1 f_3 - g_1 g_3 u\end{aligned} \tag{56}$$

where $\Lambda_3 \equiv -[\dot{g}_1(x_{3,\text{com}} - x_3) + g_1\dot{x}_{3,\text{com}} - x_{1c} - g_1\Delta^2_p]$. Let

$$u = (g_1 g_3)^{-1}[\zeta_2 + K_3\zeta_3 - g_1 f_3 + \ddot{x}_{1c} - u_{\text{ad},3}] \tag{57}$$

so that

$$\dot{\zeta}_3 = -\zeta_2 - K_3\zeta_3 + u_{\text{ad},3} - \Lambda_3 \tag{58}$$

The estimate of the aileron control effectiveness $g_3 = L_{\delta a}$ remains nonzero in most aircraft control applications. Equations (52), (55), and (58) can be now expressed in state-space form

$$\dot{\bar{\omega}} = \bar{A}\,\bar{\omega} + \bar{u}_{\text{ad}} - \bar{\Lambda} \tag{59}$$

where $\bar{\omega} \equiv [\zeta_1, \zeta_2, \zeta_3]^T$, $\bar{u}_{\text{ad}} \equiv [u_{\text{ad},1}, u_{\text{ad},2}, u_{\text{ad},3}]^T$, $\bar{\Lambda} \equiv [\Lambda_1, \Lambda_2, \Lambda_3]^T$, and

$$\bar{A} = \begin{bmatrix} -K_1 & 1 & 0 \\ -1 & -K_2 & 1 \\ 0 & -1 & -K_3 \end{bmatrix} \tag{60}$$

The gains $K_{1,2,3} > 0$ to ensure stability, but they also need to be tuned to obtain reasonable performance. The complete control policy is given by Eqs. (51), (54), and (57). For detailed proof of stability of the closed-loop system and the derivation of the adaptation law, readers are referred to [9] and the references within.

B. Turn Coordination: Adaptive Side Acceleration Control

To maintain turn coordination, the side acceleration along the y axis of the body-fixed frame a_{Y_B} is regulated to zero. The control design consists of an outer-loop proportional-integral (PI) controller acting on the side acceleration command error and whose output z_{com} is a command for the blended output $z = \beta + C_r r$ [19]. The signal z_{com} is input to an inner-loop inverting controller augmented by a single hidden layer (SHL) NN that generates the rudder deflection command δr_{com}. The details of the design are contained in [19].

C. Dynamic Inversion

From the preceding modified design for azimuth rate control and turn coordination, the equation for dynamic inversion to determine the actuator deflection commands can be set up as follows:

$$\begin{bmatrix} \ddot{R} \\ \dot{\zeta}_3 \\ \ddot{\lambda}_E - \ddot{\Theta} \\ \dot{z} \end{bmatrix} = [\bar{\Delta}_2(\bar{x}, \overline{a}_L)] + [A_2(\bar{x})] \begin{bmatrix} \delta T \\ \delta a \\ \delta e \\ \delta r \end{bmatrix} \tag{61}$$

where

$$A_2(\bar{x}) = \begin{bmatrix} -X_{\delta T}\{\cos(\Psi - \lambda_A)\cos\lambda_E \cos\Theta + \sin\lambda_E \sin\Theta\} & 0 & 0 & 0 \\ 0 & g_1(\bar{x})g_3 & 0 & 0 \\ X_{\delta T}\{\cos(\Psi - \lambda_A)\sin\lambda_E \cos\Theta - \cos\lambda_E \sin\Theta\}/R & 0 & -M_{\delta e}\cos\Phi & N_{\delta r}\sin\Phi \\ 0 & 0 & 0 & \frac{Y_{\delta r}}{U_0} + C_r N_{\delta r} \end{bmatrix} \tag{62}$$

where U_0 is the trim speed of the aircraft, the value for C_r can be obtained by following the design procedure in [19], and $\bar{\Delta}_2(\bar{x}, \overline{a}_L)$ is the modeling error vector different from the one in Eq. (25). Thus an approximate feedback linearization is given as follows:

$$\begin{bmatrix} \delta T \\ \delta a \\ \delta e \\ \delta r \end{bmatrix} = [A_2(\bar{x})]^{-1} \begin{bmatrix} \nu_R \\ \nu_{\zeta_3} \\ \nu_{\dot{\chi}_E} \\ \nu_z \end{bmatrix} \tag{63}$$

where the vector $\bar{\nu}_2 = [\nu_R \;\; \nu_{\zeta_3} \;\; \nu_{\dot{\chi}_E} \;\; \nu_z]^T$ represents the pseudocontrol input vector and represents the desired dynamics of the vector $[R, \zeta_3, \dot{\lambda}_E - \dot{\Theta}, z]^T$. The rest of the control design is very similar to the design presented in Sec. II.B.2, the details of which can be found in [16,17]. The block diagram of the overall system is shown in Fig. 3.

IV. Simulation-Based Evaluation

A. Timescale Separated Guidance and Control Design

The timescale separated guidance and control (TSSGC) design is described in complete detail in [3]. This section just provides a summary. The TSSGC design consists of an outer-loop guidance block that takes as inputs range and LOS rate commands. With feedback of LOS variables and their derivatives, and the follower aircraft kinematics state information, the guidance block computes inertial acceleration commands by carrying out approximate dynamic inversion of the range and LOS rate kinematics. The inertial acceleration commands are transformed into normal (a_{Z_B}) and longitudinal (a_{X_B}) specific force commands, and a bank angle command. These commands, along with a side acceleration command of zero, are sent to an inner-loop autopilot.

The autopilot consists of adaptive controllers for normal and side acceleration command tracking, and bank angle command tracking, plus a PI throttle controller for tracking a blend of the longitudinal acceleration and speed command V_{com}. NN-based adaptation is introduced in the guidance block to compensate for modeling error due to unknown leader aircraft acceleration. NN-based adaptation is also introduced in the autopilot to compensate for modeling error due to parametric aerodynamic modeling uncertainties.

B. Simulation Results

A nonlinear 6-DOF simulation with linearized aerodynamics is used for the testing of the control and guidance algorithms for formation flight. Quaternion attitude angles are obtained by integrating the rate gyros. The simulation model is a rigid body aircraft model with 13 states, three for position with respect to the Earth-fixed frame, three for translational velocity expressed in the body frame, four for the quaternions, and three for the angular velocity expressed in the body frame. Engine thrust is obtained from a linear interpolation map of throttle position. The actuators are modeled as first-order, stable linear filters with rate and position limits and time delays.

The IGC design 1, IGC design 2, and the TSSGC design are evaluated on the basis of tracking a commanded range from a maneuvering leader aircraft. The commanded range is 5 m, which is approximately two wingspan lengths of the follower aircraft. The LOS (bearing) rate commands for all three designs are nominally set to zero. In case the bearing angles drift to values greater than the field-of-view maximum widths, which are assumed to be ± 30 deg for both the azimuth and elevation bearing angles, the LOS (bearing) rate commands are adjusted to keep the bearing angles within ± 30 deg. The implementation of the azimuth bearing rate command $\dot{\chi}_{A,\text{com}}$ is accomplished by using the following dead-zone logic, with an almost identical logic for generating $\dot{\chi}_{E,\text{com}}$:

$$\dot{\chi}_{A,\text{com}} = \begin{cases} 0, & \text{if } |\chi_A| \le \pi/6 \\ K_{dz,\dot{\chi}_A}(\chi_A - \pi/6), & \text{if } \chi_A > \pi/6, K_{dz,\dot{\chi}_A} > 0 \\ K_{dz,\dot{\chi}_A}(\chi_A + \pi/6), & \text{if } \chi_A < -\pi/6 \end{cases} \tag{64}$$

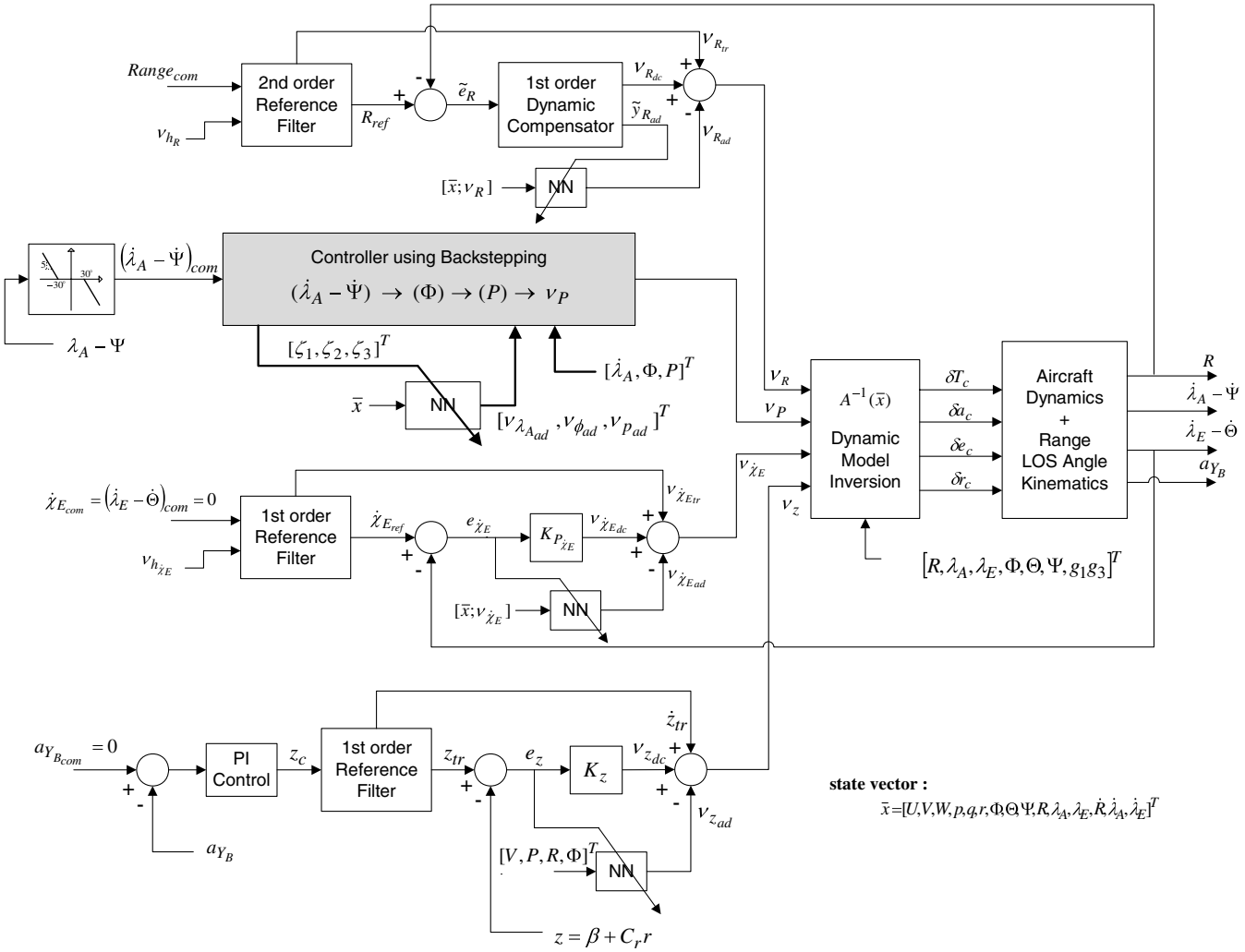

Fig. 3 Integrated guidance and control logic block diagram for follower aircraft: design 2.

The leader maneuver is a three-dimensional slanted-box maneuver as shown in Fig. 4. The commanded speed of the leader aircraft is $V_{\text{com}} = 25$ m/s. The guidance and control design for the leader aircraft is the TSSGC design outlined in Sec. IV.A. The leader starts off at the origin (0, 0, 0) and moves at constant velocity, then turns and climbs, turns again at constant altitude, and finally turns and descends to the starting point.

All of the following results include the effect of adaptation. Figure 5 shows the range command tracking performance in meters with the TSSGC, IGC-1, and IGC-2 designs. The solid line represents the commanded range $R_{\text{com}} = 5$ m, the dotted line is the range, and the dashed line represents the hedged reference signal. The range signal R tracks the hedged reference signal R_{ref}. It is clear that the performance with the IGC designs (Figs. 5b and 5c) is superior to the TSSGC design (Fig. 5a) by virtue of much smaller range overshoots (maximum of 1.5 m for the IGC designs, vs 5 m for the TSSGC design), and convergence to the commanded range in steady state. The overshoots in range occur after the leader aircraft starts a maneuver.

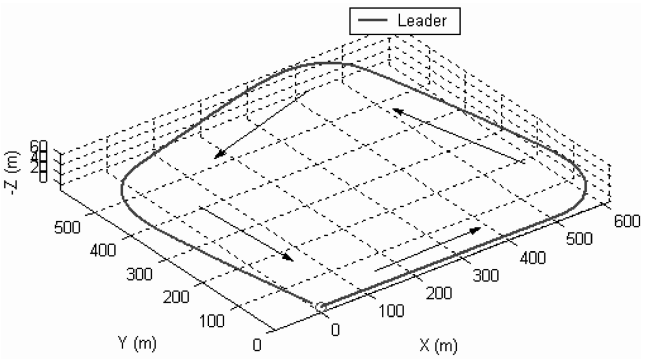

Fig. 4 Leader three-dimensional slanted-box trajectory.

One of the reasons for the deficient performance of the TSSGC design when compared with the IGC design is the choice of command to the throttle controller in the TSSGC design. The throttle controller in the TSSGC design is a PI controller with antiwindup feature. There is a stability issue if the longitudinal acceleration command $f_{x,\text{com}}$ from the guidance law is input to the throttle controller for the case of a sharply turning leader aircraft. This is due to the fact that the guidance logic generates an excessive negative acceleration command along the x axis of the body frame (highly negative $f_{x,\text{com}}$) when starting a heading turn and this causes saturation into the lower bound of the throttle, ultimately leading to instability of the entire closed-loop system. The same reasoning is applicable to the leader aircraft. And so, for the leader aircraft, the command to the throttle controller consists of only the speed command V_{com}, and for the follower aircraft, the throttle controller command is modified to be a blend of the longitudinal acceleration command $f_{x,\text{com}}$ and speed command V_{com}, given as follows:

$$\delta T_{\text{com},F} = \left(K_{p,x} + \frac{K_{I,x}}{s}\right)(V_{\text{com}} - V_F + K_x f_{x,\text{com}}) \qquad (65)$$

where $K_{p,x}$, $K_{I,x}$, and $0 \le K_x \le 1$ are design constants. This is arguably not a fair evaluation, because the follower aircraft cannot

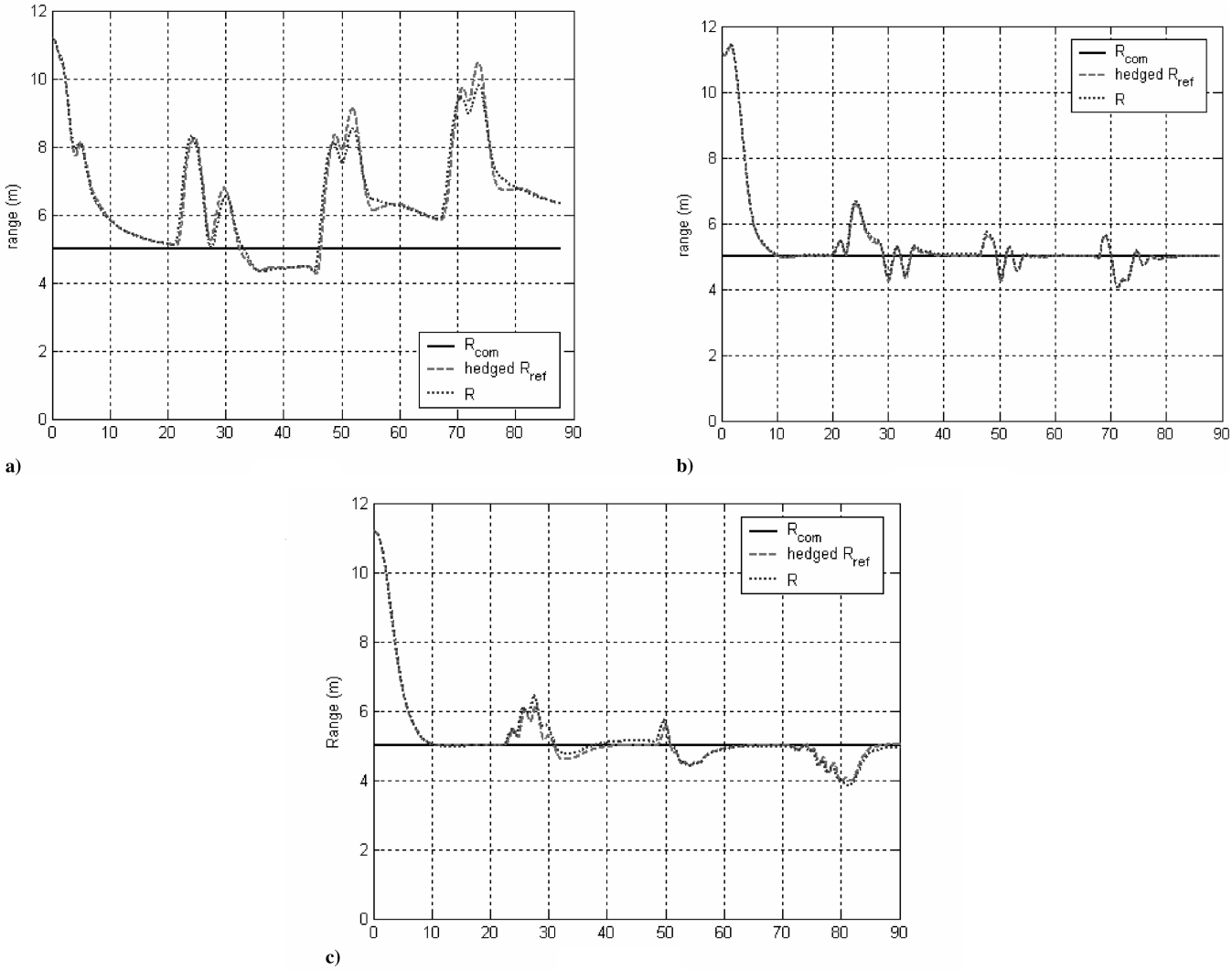

Fig. 5 Range command tracking performance, a) TSSGC design, b) IGC-1, c) IGC-2.

know a priori the commanded speed of the leader aircraft in a realistic setting. The blended throttle controller command in Eq. (65) reduces the transient speed of response of the range variable and the desired steady state with respect to range is not exactly achieved (Fig. 5a), even when the leader stops maneuvering. The consequence of the modification of the throttle command is the tradeoff between range command tracking and closed-loop stability for the TSSGC design. This is not an issue in the IGC designs because the throttle command is obtained by the dynamic inversion of the range and bearing rates' dynamics [Eqs. (28) and (63)] with adaptive compensation for the modeling errors.

Figure 6 shows the bearing rates' histories in degrees per second, and bearing angles in degrees with the TSSGC and IGC designs. When the leader maneuvers, there are large overshoots in the LOS and bearing rates' histories, but the overshoots with the IGC designs are much smaller than those with the TSSGC design. The solid lines in Figs. 6a, 6c, and 6e are the hedged reference signals. Figure 6a shows the reference signal dynamics are slower for the TSSGC design. This is because the reference model bandwidths in the TSSGC design are restricted by the limitations of the autopilot. In the IGC designs, the reference models have higher bandwidths. This is a key point of the IGC design. The IGC design allows much higher controller bandwidths than a timescale separated design, and hence can achieve better performance. In Figs. 6c and 6e, the apparent sign reversal of the reference signals is due to hedging of the IGC designs.

Figures 6b, 6d, and 6f show the bearing angles. With IGC-1 and IGC-2 designs, the bearing angles ride the boundary of the dead-zone described in Eq. (64) in the steady state with transient overshoots of less than 10 deg. With the TSSGC design, the overshoots are about 20 deg, which again show that the bearing rate regulation with the IGC designs is superior to that of the TSSGC design.

Figure 7 shows the angle-of-attack and sideslip angle histories in degrees with the TSSGC, IGC-1, and IGC-2 designs. It is clear that the sideslip angles with IGC-1 are unacceptably large (maximum 15 deg). With the TSSGC design and IGC-2, the sideslip angle histories are acceptable (maximum 4 deg).

Figure 8 shows the NN approximation of the modeling error $\bar{\boldsymbol{\Delta}}$ for the IGC-1 and IGC-2 designs. The figure shows very good approximation indicating the effectiveness of adaptation. If the adaptation is switched off, the tracking goes unstable. These results are not included.

V. Conclusions

This paper has presented an adaptive integrated guidance and control design (IGC) for formation flight using a combination of output feedback inversion and backstepping techniques. Neural-network-based online adaptation is used to compensate for modeling errors in the design process, which include uncertainties due to unknown leader aircraft acceleration, and the modeling error due to parametric uncertainties in the aircraft aerodynamic derivatives. One conclusion is that adaptation in the integrated design of guidance and flight control plays a critical role in this application. It is highly unlikely that regulation at a distance of two wingspan lengths is possible for a noncooperating maneuvering leader without adaptation. A second conclusion is that using feedback inversion

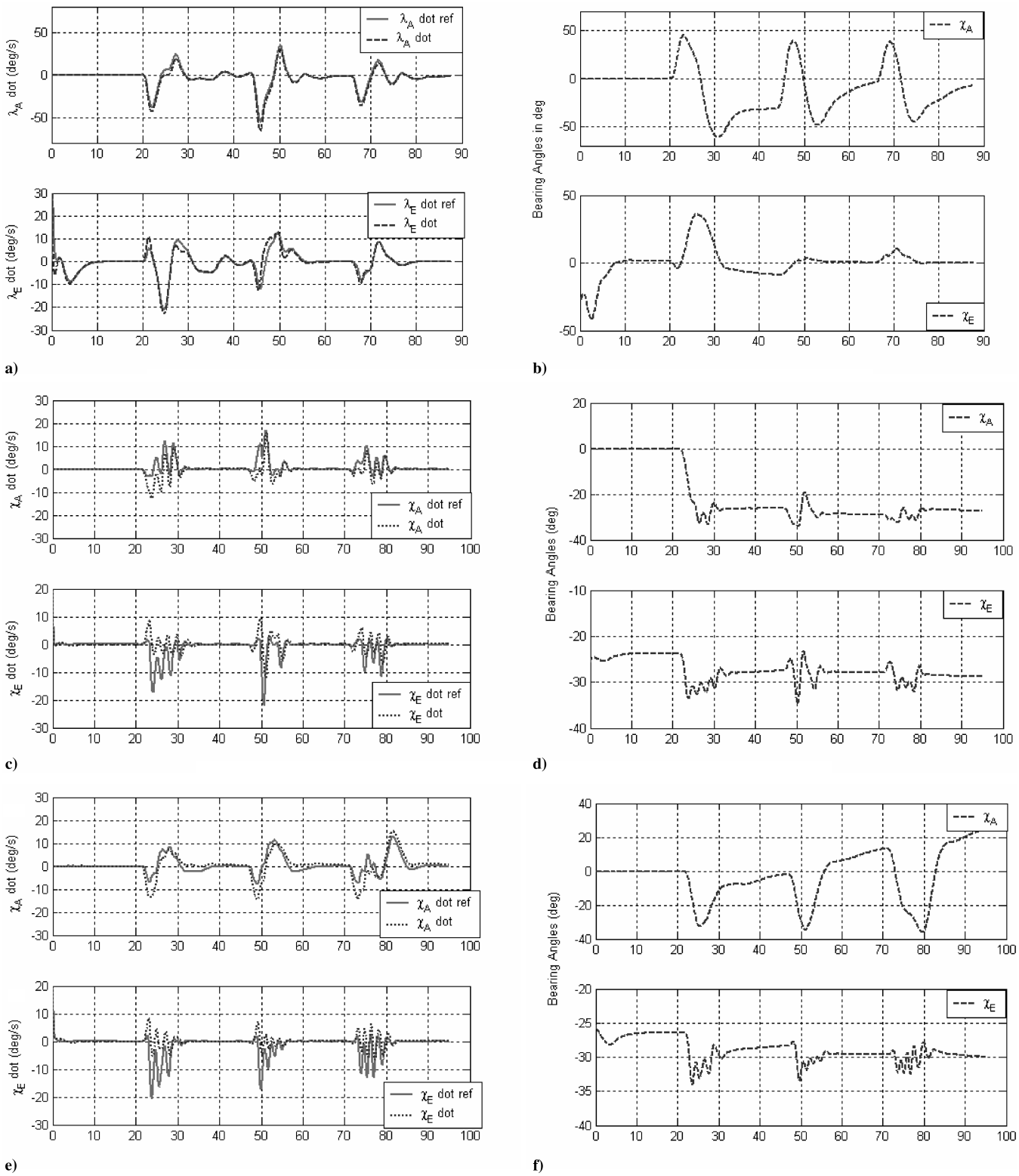

Fig. 6 Bearing rates tracking, a) TSSGC Design, c) IGC-1, e) IGC-2; bearing angles, b) TSSGC design, d) IGC-1, f) IGC-2.

alone results in a deficiency in maintaining turn coordination. This deficiency can be avoided by employing a backstepping approach for the azimuth portion of the design process. Attempting to address the full 6 DOF problem using backstepping alone leads to a cumbersome design, whereas combining feedback inversion with backstepping appears to lead to a complimentary design approach. Finally, when compared with an adaptive timescale separated guidance and control (TSSGC) design, the adaptive IGC design offers an explicit advantage of achieving a higher bandwidth design for the combined dynamics. In the case of the TSSGC design, attempting to improve the performance by increasing the bandwidth of the guidance design, while maintaining sufficient timescale separation with the autopilot design, leads to actuator saturation and eventual instability. The main advantage of the IGC design is that it translates into better transient and steady-state range tracking performance as seen in the simulation results.

Future research involves integrating the IGC design with a target-tracking estimation design and image processing followed by flight test evaluations of the complete design in vision-based formation flight of a maneuvering leader and follower aircraft.

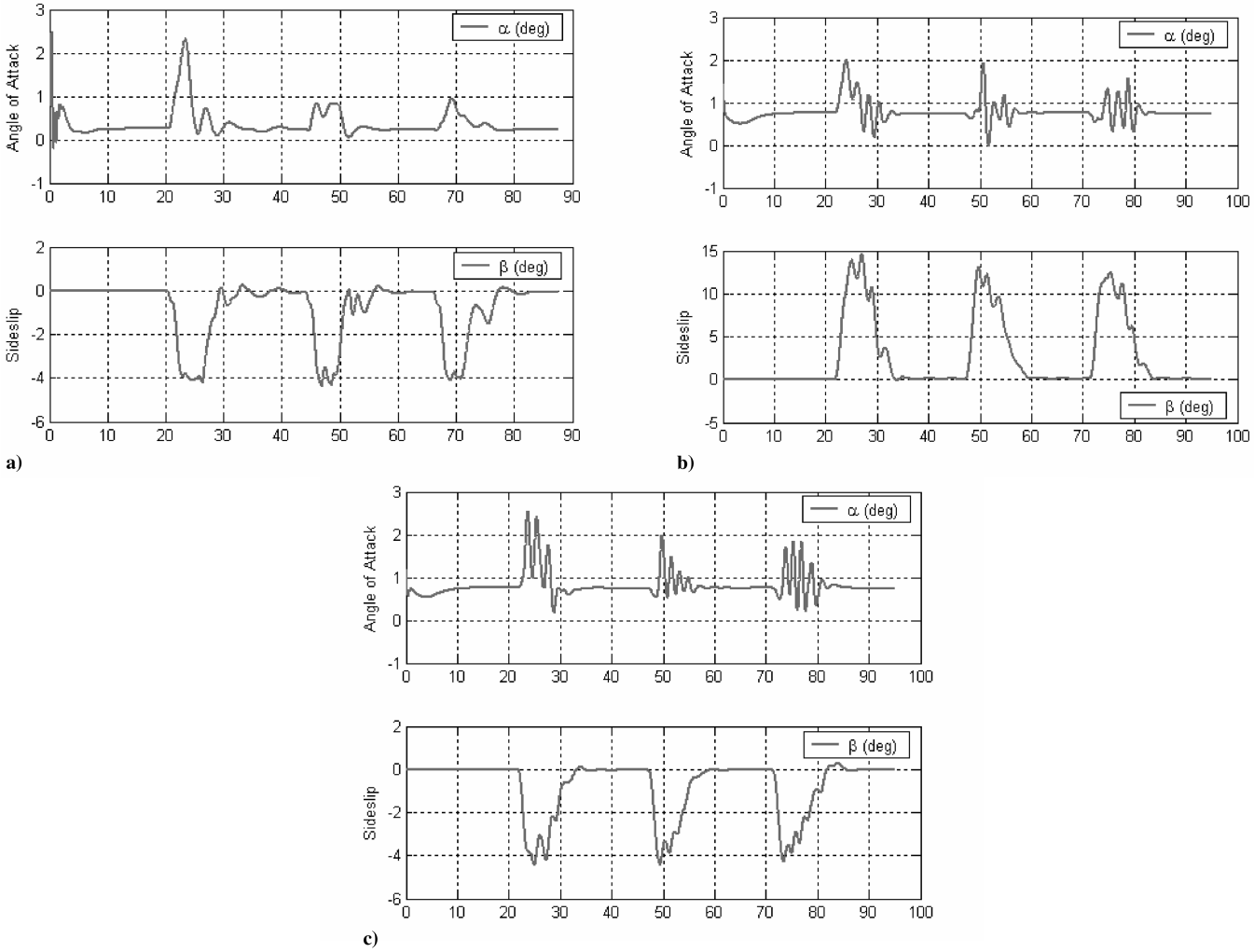

Fig. 7 Aerodynamic angles, a) TSSGC design, b) IGC-1, c) IGC-2.

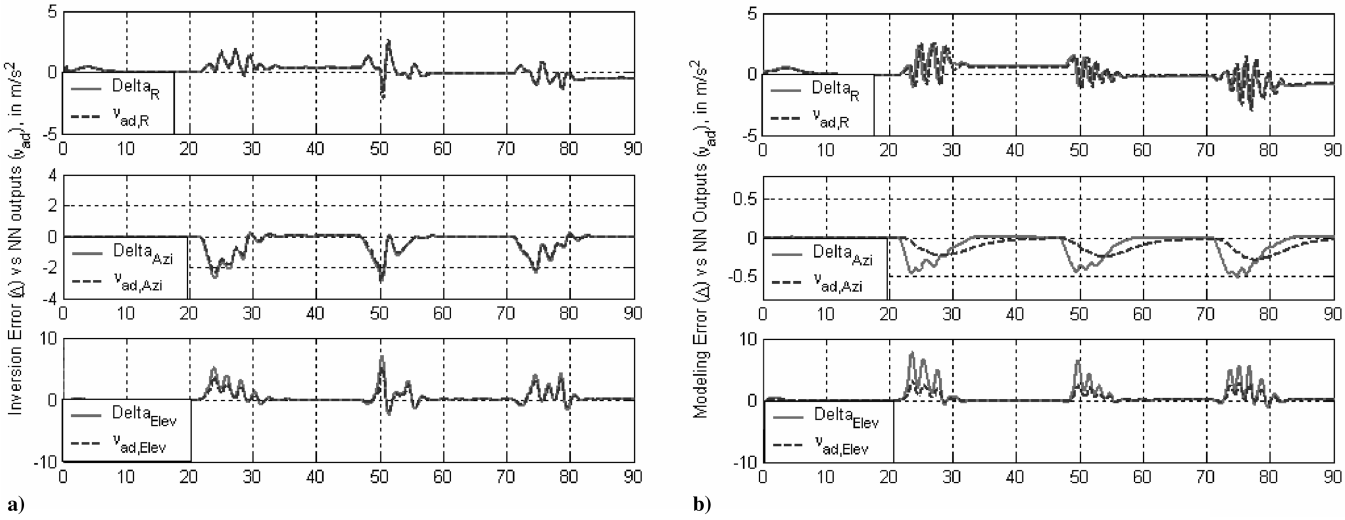

Fig. 8 Modeling error vs NN outputs ν_{ad}, a) IGC-1, b) IGC-2.

Acknowledgments

This research has been sponsored under Air Force Office of Scientific Research contract F49620-03-1-0401. The authors would particularly like to thank Johnny Evers of the U.S. Air Force Research Laboratory, Munitions Directorate, Eglin Air Force Base, Florida, for inspiring this research topic, and for his comments and collaborative efforts during the conduct of this research.

References

[1] Betser, A., Vela, P., and Tannenbaum, A., "Automatic Tracking of Flying Vehicles Using Geodesic Snakes and Kalman Filtering," *Decision and Control*, Vol. 2, Dec. 2004, pp. 1649–1654.

[2] Polloni, L., Mati, R., Innocenti, M., Campa, G., and Napolitano, M., "A Synthetic Environment for the Simulation of Vision-based Formation Flight," AIAA Paper 2003-5376, 2003.

[3] Sattigeri, R., Calise, A. J., Kim, B. S., Volyanskyy, K., and Kim, N.,

"6 DOF Nonlinear Simulation of Vision-based Formation Flight," AIAA Paper 2005-6002, 2005.

[4] Menon, P. K., and Ohlmeyer, E. J., "Integrated Design of Agile Missile Guidance and Autopilot Systems," *Control Engineering Practice*, Vol. 9, Aug. 2001, pp. 1095–1106.

[5] Menon, P. K., Sweriduk, G. D., and Ohlmeyer, E. J., "Optimal Fixed-Interval Integrated Guidance-Control Laws for Hit-to-Kill Missiles," AIAA Paper 2003-5579, 2003.

[6] Shkolnikov, I., Shtessel, Y., and Lianos, D., "Integrated Guidance-Control System of a Homing Interceptor: Sliding Mode Approach," AIAA Paper 2001-4218, 2001.

[7] Lin, C. F., Wang, Q., Speyer, J. H., Evers, J. H., and Cloutier, J. H., "Integrated Estimation, Guidance and Control System Design Using Game Theoretic Approach," *American Control Conference*, American Automatic Control Council, Evanston, IL, 1992, pp. 3220–3224.

[8] Palumbo, N. F., and Jackson, T. D., "Integrated Missile Guidance and Control: A State Dependent Riccati Differential Equation Approach," *IEEE International Conference on Control and Applications*, ISBN 0-7803-5446-X, Vol. 1, Inst. of Electrical and Electronics Engineers, New York, Aug. 1999, pp. 243–248.

[9] Sharma, M., and Richards, N., "Adaptive, Integrated Guidance and Control for Missile Interceptors," AIAA Paper 2004-4880, 2004.

[10] Krstic, M., Kanellakopoulos, I., and Kokotovic, P., *Nonlinear and Adaptive Control Design*, Wiley, New York, 1995.

[11] Johnson, E., and Kannan, S., "Adaptive Flight Control for an Autonomous Unmanned Helicopter," AIAA Paper 2002-4439, 2002.

[12] Johnson, E., and Calise, A. J., "Feedback Linearization with Neural Network Augmentation Applied to X-33 Attitude Control," *Guidance, Navigation and Control Conference*, AIAA Paper 2000-4157, Aug. 2000.

[13] Johnson, E., Calise, A., Sattigeri, R., Watanabe, Y., and Madyastha, V., "Approaches to Vision-Based Formation Control," *43rd IEEE Conference on Decision and Control*, Vol. 2, Dec. 2004, pp 1643–1648.

[14] Isidori, A., *Nonlinear Control Systems*, Springer–Verlag, Berlin, 1989.

[15] Etkin, B., *Dynamics of Atmospheric Flight*, Wiley, New York, 1972.

[16] Calise, A. J., Hovakimyan, N., and Idan, M., "Adaptive Output Feedback Control of Nonlinear Systems Using Neural Networks," *Automatica*, Vol. 37, No. 8, 2001, pp. 1201–1211.

[17] Hovakimyan, N., Calise, A. J., and Kim, N., "Adaptive Output Feedback Control of a Class of Multi-Input Multi-Output Systems using Neural Networks," *International Journal of Control*, Vol. 77, No. 15, Oct. 2004, pp. 1318–1329.

[18] Narendra, K., and Annaswamy, A., *Stable Adaptive Control*, Prentice–Hall, Upper Saddle River, NJ, 1995.

[19] Calise, A. J., Sharma, M., and Corban, E. J., "Adaptive Autopilot Design for Guided Munitions," *Journal of Guidance, Control, and Dynamics*, Vol. 23, No. 5, Sept.–Oct. 2000, pp. 837–843.